Application of SiO$_2$ passivation technique in mass production of silicon solar cells

Y.F. Zhuang[a], S.H. Zhong[a], X.J. Liang[b], H.J. Kang[b], Z.P. Li[a], W.Z. Shen[a,c,*]

[a] *Institute of Solar Energy, and Key Laboratory of Artificial Structures and Quantum Control (Ministry of Education), Department of Physics and Astronomy, Shanghai Jiao Tong University, Shanghai 200240, People's Republic of China*
[b] *Shanghai Shenzhou New Energy Development Co., Ltd., Shanghai 201112, People's Republic of China*
[c] *Collaborative Innovation Center of Advanced Microstructures, Nanjing 210093, People's Republic of China*

ARTICLE INFO

ABSTRACT

Effective surface passivation is one of the primary prerequisites for high-efficiency silicon solar cells. In this paper, high-quality silicon dioxide (SiO$_2$) films with excellent surface passivation abilities have been realized by thermal oxidation and plasma-enhanced chemical vapor deposition, respectively. By employing SiO$_2$ capped with hydrogenated silicon nitride (SiN$_x$:H) (SiO$_2$/SiN$_x$:H stacks) as the front passivation layers, the emitter saturation current density has been reduced from 90.5 fA/cm^2 to 62.3 fA/cm^2. We have successfully mass-produced thermal-oxidized p-type Czochralski-Si (CZ-Si) solar cells with high conversion efficiency (η) of 20.1%, which is 0.2% absolutely higher than that of the conventional Al back surface field (Al-BSF) solar cells. With a rational design of process integration, we have further presented a cost-effective way to fabricate high-efficiency SiO$_2$ passivated emitter and rear cells (PERCs) at an existing production line. The introduction of SiO$_2$/SiN$_x$:H stacks on the rear surface can effectively increase the long wavelength response and the rear surface recombination is also suppressed with a rather low surface recombination velocity of 26 cm/s achieved after a post-annealing process. The industrial SiO$_2$ passivated p-type CZ-Si PERCs possess outstanding performances with the average η of 21.3% and the highest η of over 21.9%, absolute 1.3% increment in average η compared with the conventional Al-BSF solar cells. Moreover, we have demonstrated that the relative low illumination response (below 50 W/m^2) loss of our SiO$_2$ PERCs over a day is extremely limited to be less than 0.2%.

1. Introduction

Although silicon based solar cells have developed rapidly in the last decade, the photovoltaic (PV) industry still occupies a rather low market share, compared with that of the conventional coal power industry. There are lots of works lying ahead for us to reduce solar energy cost and realize grid parity. Enhancement in the conversion efficiency (η) of silicon solar cells with low cost is one of the most important tasks in reduction of levelized cost of electricity in the PV industry. To achieve high-efficiency silicon solar cells, a high level of surface passivation is a prerequisite. Passivated emitter and rear cell (PERC) [1], which possesses excellent rear surface passivation, has been redeveloped rapidly in the past few years. Recent researches demonstrated that aluminum oxide (Al$_2$O$_3$) capped by hydrogenated silicon nitride (SiN$_x$:H) is a promising candidate for the rear surface passivation of industry-dominated p-type silicon solar cells [2–5]. The

impressive passivation properties of Al$_2$O$_3$ is related to the combination of a reasonable chemical surface passivation with a low interface trap density and a field-effect passivation generated from a high density of fixed negative charges [6–8]. Industrially relevant deposition techniques for Al$_2$O$_3$ are atomic layer deposition (ALD) and plasma-enhanced chemical vapor deposition (PECVD). Huang et al. [9] have reported industrial Al$_2$O$_3$ PERCs with η of 20.8%. Although ALD and the developed PECVD [10] devices have already been employed in some new production lines in the current PV industry, the introduction of the new devices to the existing production lines maybe not lucrative. It may take a long time and a high cost to integrate the new devices and the old ones to achieve a high compatibility. Moreover, the trimethylaluminum (TMAl) precursor material is also costly.

The high-efficiency p-type silicon solar cells should also feature a low recombination at the front surface. SiN$_x$:H film is well known for its good antireflection properties and is widely used in the silicon solar
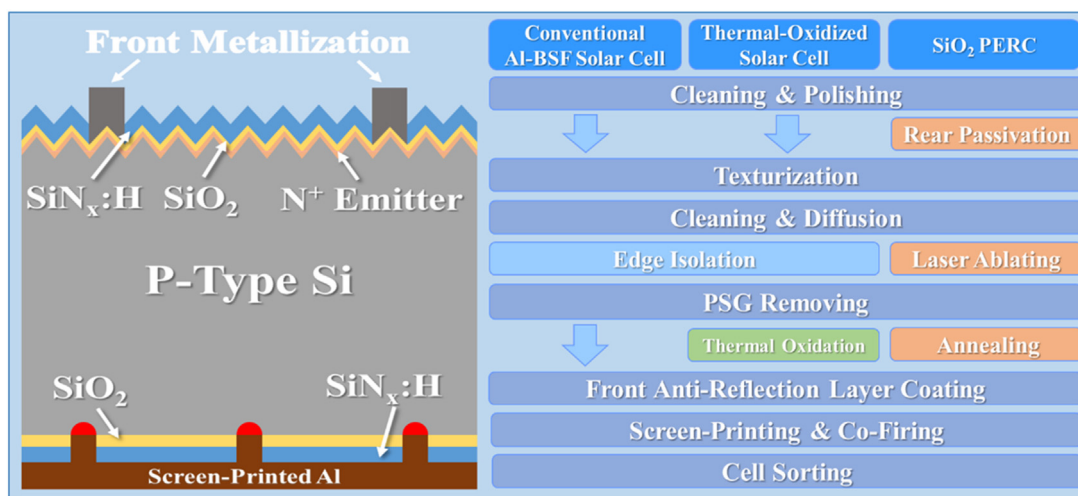

Fig. 1. Schematic illustration of the main steps for the fabrication (right) of the silicon solar cells, together with the diagram of the SiO$_2$ PERC structure (left).

cells as a front surface antireflection coating (ARC) layer [11]. Nevertheless, the passivation effect of SiN$_x$:H films is inadequate [12]. Although the Al$_2$O$_3$/SiN$_x$:H stack films perform excellent passivation effect on silicon surfaces, they are not suitable for passivating the front n$^+$ emitter of p-type silicon solar cells as an inversion layer will be formed. The inversion layer is associated with a lifetime reduction at low injection levels [13–15]. Moreover, it acts a sun desired conduction pathway to metal contacts, depressing the solar cell performance via the open circuit voltage (V_{OC}), short circuit current (I_{SC}) and fill factor (FF).

Another candidate for the silicon surface passivation dielectric films is silicon dioxide (SiO$_2$) and SiN$_x$:H stacks (SiO$_2$/SiN$_x$:H). Literatures reported that a SiO$_2$ layer helps to improve the passivation quality of a textured front surface with emitters for both n- and p-type silicon surfaces, as well as the rear surfaces [16–21]. The SiO$_2$ layer can effectively passivate the dangling bonds on the Si surface and a low surface recombination velocity (S_{eff}) (~ 30 cm/s) is achieved after a post-annealing process [18]. Additionally, SiO$_2$ layers can be either grown by liquid phase deposition (LPD), ALD, thermal oxidation, PECVD and chemical oxidation processes [7,16,19–22]. Among them, thermal oxidation and PECVD techniques are very promising for mass production considering the cost-effectiveness and the compatibility with the existing production line. By employing these methods, Gatz et al. [23] and Munzer et al. [24] have developed industrial feasible PERC fabrication processes, respectively. However, the promotion of the SiO$_2$ passivation techniques in the industry is extremely limited, which may be mainly due to the reduced response at low illumination levels [25] and the limited η enhancement of SiO$_2$ passivated solar cells.

In this study, we have successfully developed industrial feasible SiO$_2$ passivation techniques based on the existing production lines. By employing thermal oxidization SiO$_2$ capped with PECVD SiN$_x$:H as the front passivation layers, the emitter saturation current density (J_{0e}) on the front surface has been reduced from 90.5 fA/cm^2 to 62.3 fA/cm^2. The average η of the fabricated thermal-oxidized p-type CZ-Si solar cells reaches 20.1%, which is 0.2% absolutely higher than that of the conventional Al back surface field (Al-BSF) solar cells. In addition, we have presented a cost-effective way to fabricate high-efficiency SiO$_2$ PERCs by PECVD, which is highly compatible with the existing production lines. By introducing SiO$_2$/SiN$_x$:H layers on the rear surface, a low S_{eff} of 26 cm/s is achieved. The industrial SiO$_2$ PERCs exhibit high performances with average V_{OC} of 657 mV, I_{SC} of 9.86 A and η of 21.3%. Compared with the conventional Al-BSF solar cells, absolute 1.3% increment in η is achieved and the highest η of our SiO$_2$ PERCs reaches 21.9%. Moreover, via a careful calculation with considering the variation of solar spectrum with time, relative low illumination response

(below 50 W/m^2) loss of our SiO$_2$ PERCs over a day is expected to be less than 0.2%, which is a great importance in the real application.

2. Experimental and simulation

P-type Czochralski-Si (CZ-Si) wafers with a size of pseudo square 156.75 × 156.75 mm^2 and p-type diamond wire sawn (DWS) mc-Si with a size of 156.75 × 156.75 mm^2, a thickness of 180 ± 10 μm and resistivity of 1–3 Ω·cm were used for this work.

2.1. Surface textures

For the CZ-Si wafers, industrial texturing method was followed, namely, silicon wafers were etched in an alkaline solution containing 1.1% NaOH and 8 vol% IPA under the solution temperature of 83 °C for 30 min. The surface texturing for the mc-Si wafers was produced in a production line by employing a black silicon method, which has been detailed in our previous research [26]. After the texturing processes, industrial cleaning processes were employed to remove metal ion contamination and oxide layer.

2.2. Fabrication of solar cells

The solar cell fabrication processes are shown in Fig. 1. For conventional Al-BSF solar cells, the textured wafers underwent a standard industrial solar cell fabricating process, including n-type diffusion with POCl$_3$ as diffusion source (M5111-4WL/UM, CETC 48th Research Institute), edge isolation in HF/HNO$_3$ solution (InOxSide, RENA), removal of the phosphorous silicate glass (PSG) in dilute HF solution (InOxSide, RENA), deposition of double SiN$_x$:H layers on the front surface by PECVD system (M82200-6/UM, CETC 48th Research Institute), the fabrication of front and back electrodes by screen printing technique (PV1200, DEK) and co-firing process (CF-Series, Despatch). The composite refractive index of the double SiN$_x$:H layers was 2.05 at 632.1 nm while the refractive index of the bottom SiN$_x$:H layer was 2.18.

For thermal-oxidized solar cells, the wafers underwent the above-mentioned standard industrial solar cell fabricating process together with a thermal oxidation process by a Centrotherm diffusion furnace (E2000) at 700 °C for 60 min with two steps after removing the PSG. The gas flow rates of N$_2$ and O$_2$ were 5 slm and 2 slm at the first step while they were 6 slm and 1 slm at the second step. The thickness of the SiO$_2$ layer was nearly 2 nm. The composite refractive index of the double SiN$_x$:H layers was 2.05 at 632.1 nm while the refractive index of the bottom SiN$_x$:H layer was 2.15.

For SiO$_2$ PERCs, firstly, the stack SiO$_2$/SiN$_x$:H passivation layers were deposited on the rear surface by PECVD at 450 °C after alkali etching. The thickness of SiO$_2$/SiN$_x$:H stacks ranged from 0 to 300 nm. After the texturization process, n$^+$-emitter was formed on the front surface during the diffusion process for about 100 min at 800 °C. After that, local line openings were formed by laser ablating (DR-LA-Y40, DR Laser), followed by the PSG removing process and an annealing process at 700 °C for 30 min. The gas flow rate of N$_2$ was 12 slm during the annealing process. Then the stack SiO$_2$/SiN$_x$:H passivation layers were deposited on the front surface by PECVD. Finally, the wafers underwent the conventional screen printing and the co-firing processes.

2.3. Fabrication of the samples for recombination comparison

For the study of J_{0e}, SiN$_x$:H passivation layers (conventional AL-BSF samples) and stack SiO$_2$/SiN$_x$:H passivation layers (thermal-oxidized samples) were deposited on both surfaces of the textured and diffused wafers. After that, the wafers underwent the conventional sintering process without metallization.

For the study effective minority carrier lifetime (τ_{eff}) of SiO$_2$ PERCs, stack SiO$_2$/SiN$_x$:H passivation layers were deposited on both surfaces of polished wafers, followed by an annealing process in air atmosphere at 500–800 °C for 30 min. The τ_{eff} was measured at the injection density of 1×10^{15} cm^{-3}.

2.4. Characterization

The morphologies of the wafers were investigated by field emission scanning electron microscopy (FE-SEM) (Zeiss Ultra Plus). The reflectance and quantum efficiencies of the solar cells were measured by QEX10 (PV Measurements) system. Quantum efficiencies varying with illumination intensity were measured by Enlitch-S6. Refractive index and thickness of the SiN$_x$:H layers were measured by an ellipsometer device (SE400PV). Dopant concentration profiles of the phosphorus emitters were measured by electrochemical capacitance voltage (ECV) profiling (CVP21, WEP). Sheet resistance was measured by fourpoint probes (280I Series, Four Dimensions Inc.) And the electrical parameters of the solar cells were measured under AM1.5 spectrum at the temperature of 25 °C.

2.5. Simulation of current loss

The simulations of current loss were carried out by Cell Doctor software developed by Solar Energy Research Institute of Singapore (SERIS) based on the measured reflectance and quantum efficiencies of the solar cells.

2.6. Simulation of optical absorption in Al-BSF

The simulations of optical absorption in Al back surface field (Al-BSF) were carried out by the online wafer ray tracer (PV Lighthouse). Stack SiO$_2$/SiN$_x$:H layers were set on both surfaces of the silicon substrate. The thickness of the stack layers at the front surface was 80 nm while it varied 0–450 nm at the rear surface. Pure Al layer was treated as the Al-BSF in our cases, and the thickness of Al layer was 2 μm, which guaranteed that no light can transmit through it.

2.7. Simulation of electrical field intensity

The electrical field intensity was numerically calculated by Lumerical finite difference time domain (FDTD) software. The silicon substrate thickness was set to be 10 μm. A single pyramid with a lateral size of 4 μm was located at the front surface of silicon substrate. A 80 nm thick SiN$_x$:H layer was covered on the surface of the pyramid and 250 nm thick SiO$_2$/SiN$_x$:H stack layers was located at the rear surface of silicon substrate. While 200 nm thick Al layer was set at the bottom of

the rear SiO$_2$/SiN$_x$:H stack layers. The refractive index of Si, SiO$_2$, SiN$_x$:H and Al were acquired from the website of PV lighthouse. Bloch boundary in the x-y region and perfectly matched layers (PML) boundary in the z-direction was adopted in our case. The light source was a plane wave with a fixed wavelength of 750 and 1150 nm. The polarization angle was set to be 45°, which will lead to the simulated results the same with averaging those of P polarization and S polarization.

2.8. Simulation of solar spectrum

The solar spectrum irradiances under clear-sky conditions at different dates and time were obtained by solar spectrum calculator on the website of PV lighthouse. The module location was assumed to be in Shanghai, namely latitude of 31° and longitude of 121°.

3. Result and discussion

3.1. Front surface passivation by SiO$_2$/SiN$_x$:H stacks

To evaluate the passivation effect of SiO$_2$/SiN$_x$:H stacks after formation the emitter (the dopant concentration profiles of the emitters are shown in Fig. S1 in the Supplementary information), we have carried out the calculation of J_{0e} based on the following equation [27]:

$$\frac{1}{\tau_{eff}} - \frac{1}{\tau_{Auger}} = \frac{1}{\tau_{SRH}} + \frac{2J_{0e}}{qn_i^2 D}(N_{dop} + \Delta n) \tag{1}$$

where τ_{Auger} and τ_{SRH} respectively represent the carrier lifetime related to Auger recombination and Shockley-Read-Hall recombination, q the electron charge, n_i the intrinsic carrier density, D the wafer thickness (≈ 170 μm in our cases), N_{dop} the doping concentration of the substrate and Δn the excess carrier density. Through the linear fit of $(1/\tau_{eff} - 1/\tau_{Auger})$ with respect to the Δn, as shown in Fig. 2a, J_{0e} is calculated to be 62.3 fA/cm^2 for the thermal-oxidized samples, much lower than that of 90.5 fA/cm^2 for the reference sample. The lower J_{0e} of the thermal-oxidized sample means lower carrier recombination at the front surface and suggests a higher V_{OC}.

In order to evaluate how the SiO$_2$ passivation affects the solar cell performances, we have compared the measured reflectance and internal quantum efficiency (IQE) spectra of the fabricated thermal-oxidized solar cells and the conventional Al-BSF solar cells, as illustrated in Fig. 2b. The reflectance spectra of the two samples are nearly overlapped over the whole wavelength range, suggesting that the SiO$_2$/SiN$_x$:H stacks little affect the optical absorption of the solar cells. While the modified sample exhibits a higher IQE in the short wavelength range from 300 to 500 nm (shown in the zoomed-in figure), indicating that a better front surface passivation is achieved.

To further reveal the mechanism behind the results, we have carried out the simulation of current loss based on the measured reflectance and IQE data, as shown in Fig. 2c. Obviously, there is little difference in base collection loss, parasitic absorption, front surface escape and ARC reflectance loss of the modified sample and the counterpart, while blue loss is significantly suppressed in our modified sample with a value of 0.08 mA/cm^2, which is 10% less than that in the counterpart. Note that blue loss is a combined loss of recombination in the emitter and front surface recombination. These results clearly demonstrate that the SiO$_2$ layer provides a considerable chemical passivation effect on Si surfaces and well plays the role of transition layer between SiN$_x$:H layer and silicon substrate, which is consistent with the results illustrated in Fig. 2a.

3.2. Application of SiO$_2$/SiN$_x$:H stacks in the mass production of Al-BSF cells

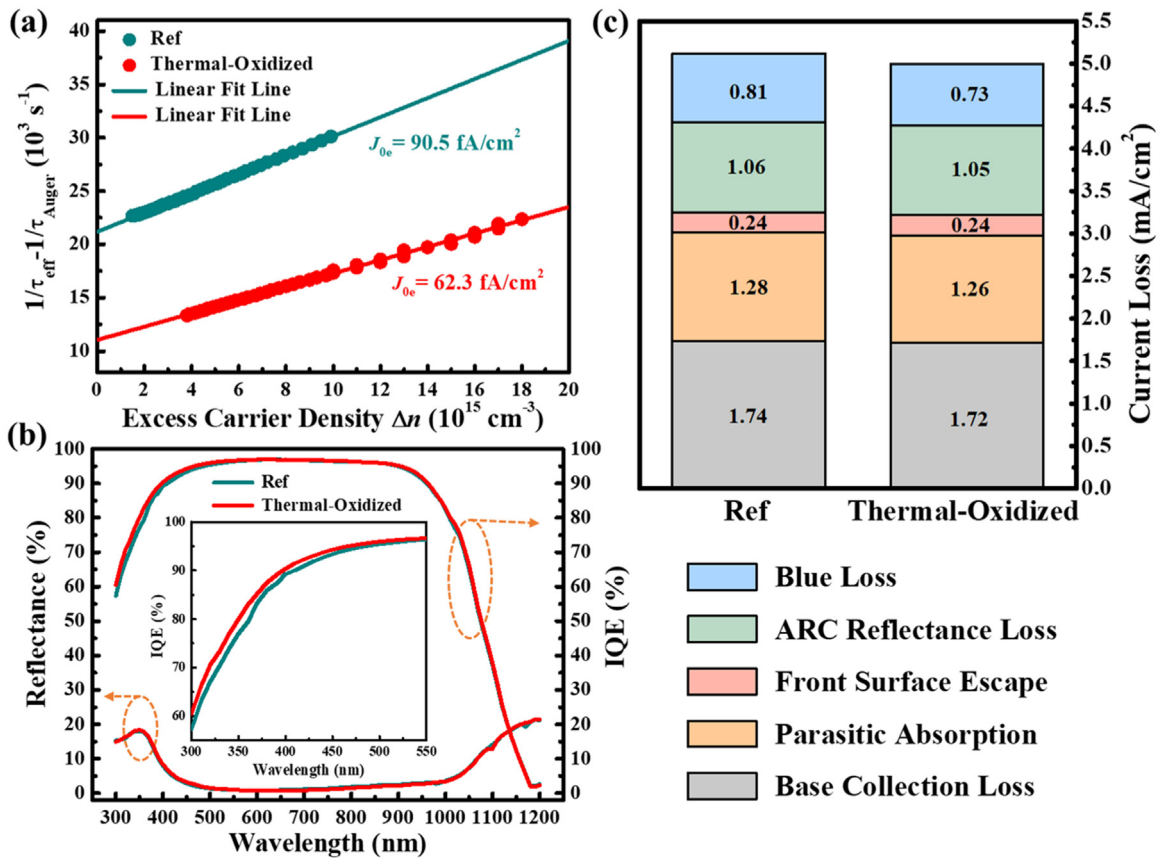We have further applied the SiO$_2$/SiN$_x$:H passivation technique in

Fig. 2. (a) Comparison of $(1/\tau_{eff} - 1/\tau_{Auger})$ of the thermal-oxidized (SiO_2/SiN_x:H passivated) and the reference (SiN_x:H passivated) samples, which are double side textured and diffused. (b) Experimental reflectance and IQE spectra (300–1200 nm). (c) Simulated current loss of the fabricated solar cells.
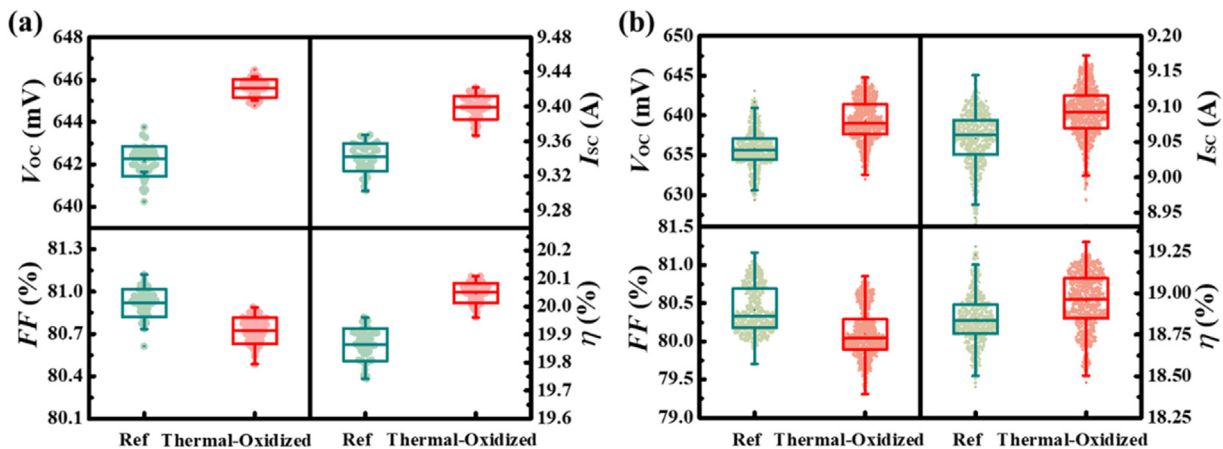

Fig. 3. Measured *I-V* parameters of (a) thermal-oxidized CZ-Si solar cells against the reference counterparts and (b) thermal-oxidized mc-Si solar cells against the reference counterparts.

the mass production of Al-BSF cells. Fig. 3a presents the distribution of the measured current-voltage (*I-V*) parameters including open circuit voltage V_{OC}, short circuit current I_{SC}, fill factor *FF* and efficiency η of the thermal-oxidized CZ-Si solar cells against the conventional Al-BSF counterparts (reference). Apparently, the performances of the thermal-oxidized solar cells exceed the reference ones significantly. Compared with the reference solar cells, the average V_{OC} of the thermal-oxidized solar cells is much higher with an absolute increment value of 3.5 mV, reaching 645.6 mV. Meanwhile, higher I_{SC} with the average value of 9.40 A is also achieved, which is 60 mA absolutely higher than that of reference solar cells. Although there is a little decrease in *FF*, the average η of the thermal-oxidized solar cells reaches 20.1%, possessing

an absolute increase of 0.2% over the reference solar cells with the average η of 19.9%. Moreover, we have further mass-produced (~1000 pieces) mc-Si solar cells based on the thermal oxidation technique. The distribution of the parameters V_{OC}, I_{SC}, *FF* and η of the thermal-oxidized solar cells against the reference solar cells are shown in Fig. 3b. Obviously, similar trend is also observed in mc-Si solar cells. By employing SiO_2/SiN_x:H passivation on the front surface, the thermal-oxidized mc-Si solar cells exhibit high performances with V_{OC} of 639.3 mV and I_{SC} of 9.09 A. And the average η reaches 19.0%, which is 0.1% absolutely higher than that of the reference counterparts. These results presented above demonstrate that SiO_2/SiN_x:H passivation can effectively enhance the solar cell performances no matter whether CZ-Si or mc-Si
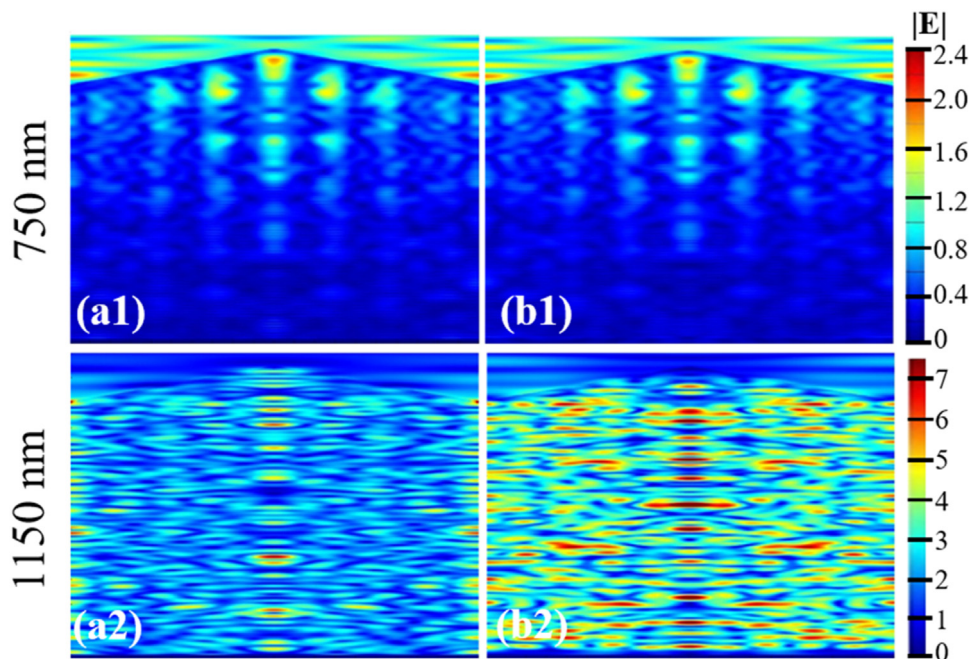
Fig. 4. Electric field distributions in the silicon substrate without (a1&a2) and with (b1&b2) SiO_2/SiN_x:H stacks on the rear surface at the incident wavelength of 750 and 1150 nm, respectively.

solar cells.

3.3. Rational design of the rear surface

Based on the results presented above, we have successfully improved the front surface passivation and the spectral response of the solar cells in the short wavelength range by the introduction of SiO_2/SiN_x:H stacks on the front surface. However, to realize high-efficiency silicon solar cells, it is also very important to improve the solar cell properties in the long wavelength range by the rational design of the rear surface. PERCs, which introduce a dielectric passivation layer on the rear surface, can effectively enhance the longwave response of the solar cells. SiO_2/SiN_x:H stacks were employed in our cases and systematic investigation was carried out.

Here, we have studied the electric field distributions in the conventional Al-BSF cell (Fig. 4 a1&a2) and our design (SiO_2/SiN_x:H stacks on the rear surface) (Fig. 4 b1&b2) at the incident light wavelength of 750 and 1150 nm, respectively. Note that shortwave light (< 950 nm) can be easily absorbed at the front surface. As a result, the resonance behaviors remain the same whatever the rear surface changes (Fig. 4 a1 &b1). When the incident wavelength is increased (i.e., 1150 nm), the incident light cannot be totally absorbed by the silicon substrate due to limited thickness and thus multiple inner reflection occurs (Fig. 4 a2& b2). Obviously, the electric field distribution in our design is much stronger, compared with that in the conventional Al-BSF cell. The results reveal that the rear SiO_2/SiN_x:H layers act as an inner reflector and more longwave light can be reflected back to the silicon substrate, which is beneficial to longwave spectral response of solar cells.

To further understand how the SiO_2/SiN_x:H stacks affect the longwave properties, we have carried out the simulation of the longwave absorption in Al-BSF with rear SiO_2/SiN_x:H stacks varying from 0 to 450 nm, as shown in Fig. 5a. The optical absorption in Al-BSF decreases rapidly with increasing thickness of the SiO_2/SiN_x:H layers. And it reaches the minimum for SiO_2/SiN_x:H thickness of more than 200 nm, which is owing to less penetration of evanescent waves and the diminishing parasitic absorption in Al-BSF [28]. Therefore, more light in long wavelength can be reflected back into the silicon substrate and increased optical absorption in silicon substrate is achieved.

In the real production, the planeness of the rear surface is of great importance, which can be evaluated by measuring the surface reflectance. Fig. 5b displays the averaged reflectance of the rear surface with different etching processes. Note that conventional acid etching with the weight reduction of 0.15 g is employed in the production line. Evidently, alkali etching presents preferable surface etching behaviors compared with acid etching, when the weight reduction of the silicon substrate is over 0.15 g. More importantly, alkali etching is 70% cost less than acid etching, and shows better environment performance [29]. Note that 0.3 g is the appropriate weight reduction value in our cases, which satisfies the planeness requirement, as well as the production cost. The SEM image of the 0.3 g alkali etched sample is shown in the inset of Fig. 5b. The size of the pyramid base is over 20 μm and the averaged surface reflectance reaches 50%.

Based on the optimized rear surface etching, we have investigated the optical behaviors of the silicon wafers with the introduction of SiO_2/SiN_x:H layers on the rear surface, as shown in Fig. 5c. With increasing the thickness of SiO_2/SiN_x:H layers on the rear surface, the longwave reflectance increases dramatically and finally reaches the maximum (about 55% at 1200 nm). These results are consistent with the simulation results shown in Fig. 5a. Considering the cost-effectiveness, SiO_2/SiN_x:H layers with ~ 15 nm SiO_2 and ~ 85 nm SiN_x:H on the rear surface are adopted in our cases.

Besides the increased optical absorption in silicon substrate, SiO_2/SiN_x:H layers can also effectively passivate the silicon surface to suppress the electrical losses of the solar cells after an annealing process. Fig. 5d illustrates the influence of different annealing temperatures on the τ_{eff} of the passivated silicon substrate. Compared with the acid etched sample, the alkali etched one exhibits a higher τ_{eff} (~ 210 μs). Furthermore, the surface passivation ability of the SiO_2/SiN_x:H stacks can be further improved by a post-annealing process. The τ_{eff} of the post-annealed samples are much higher than those of the as-deposited ones, and reaches the maximum of 275 μs at the optimized annealing temperature of 700 °C. This improved τ_{eff} may be attributed to the reconstruction of the Si/SiO_2 interface which makes the dangling bonds on Si wafer surface effectively passivated and the H passivation released from SiN_x:H [30], resulting in a low S_{eff} of 26 cm/s, which is determined by the following equation [31]:
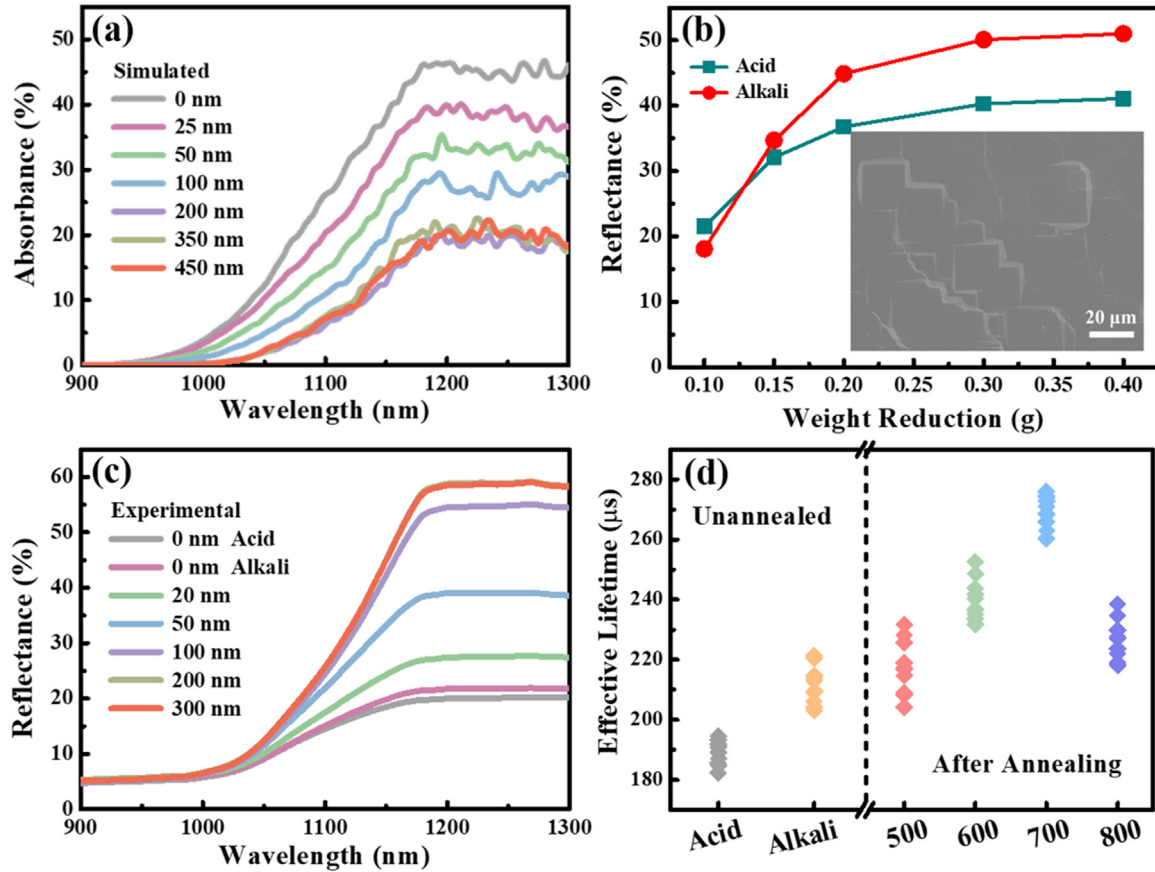
Fig. 5. (a) Simulated optical absorption in Al-BSF with SiO_2/SiN_x:H stack layers deposited on the rear surface. (b) Averaged reflectance of the rear surface with different etching processes. (c) Experimental reflectance spectra of the solar cells with SiO_2/SiN_x:H stacks deposited on the rear surface. (d) Measured τ_{eff} with respect to different annealing temperatures.

$$\frac{1}{\tau_{eff}} = \frac{1}{\tau_{bulk}} + \frac{2S_{eff}}{D} \tag{2}$$

where τ_{bulk} presents the bulk recombination lifetime. Here, we only consider the intrinsic τ_{bulk} according to the formula by Richter et al. [32], and thus the calculated S_{eff} represents the upper limit of the surface recombination velocity.

3.4. 21.3% industry SiO_2 PERCs

By employing SiO_2/SiN_x:H stacks as the passivation layers for both the front and rear surfaces, we have mass-produced SiO_2 PERCs in a production line. We compare the reflectance, external quantum efficiency (EQE) spectra and *I-V* parameters of the SiO_2 PERCs with those of the conventional Al-BSF solar cells in Fig. 6. As shown in Fig. 6a, owing to the excellent surface passivation effect by SiO_2/SiN_x:H stacks and the suppressed penetration of evanescent waves, our SiO_2 PERCs exhibit higher EQE in both short and long wavelength ranges, demonstrating a stronger spectral response.

Fig. 6b illustrates the measured output parameters including V_{OC}, I_{SC}, *FF* and η of the industrial SiO_2 PERCs and the conventional solar cells (about 10,000 pieces for each group). Compared with the conventional Al-BSF counterparts, the average V_{OC} of SiO_2 PERCs is much higher with an absolute increment value of 17 mV, reaching 657 mV. The result suggests that the passivation for the both surfaces of the silicon substrate by SiO_2/SiN_x:H stacks effectively suppresses the electrical losses. In addition, owing to the enhanced spectral response in both short wavelength and long wavelength, high I_{SC} with the average value of 9.86 A is achieved, which is 0.46 A absolutely higher than that of the conventional Al-BSF counterparts. Resulting from the high

performance of V_{OC} and I_{SC}, we have successfully produced high-efficiency industrial SiO_2 PERCs with an average η of 21.3%. Compared with the conventional Al-BSF solar cells, absolute η increment of about 1.3% is achieved. Furthermore, the η distribution of the solar cells is presented in Fig. 6c. The result shows that there is a lot of room for improvement during the fabrication processes of SiO_2 PERCs and the average η can be further enhanced. Fig. 6d shows the *I-V* characteristics of the best SiO_2 PERC and the best conventional Al-BSF solar cell. The highest η of our SiO_2 PERCs reaches 21.9% and the maximum output power is 5.36 W on the wafer size of 244.32 cm^2, which is 0.39 W absolutely higher than that of conventional Al-BSF solar cell.

3.5. Excellent behaviors at low solar irradiance

In the real application, with the rotation of the earth, it is also highly necessary to understand the solar cell performances over different solar irradiances, which is relevant to the electric energy generation. We have measured the EQE of our SiO_2 PERCs by varying the solar irradiance, as illustrated in Fig. 7a. It can be seen that the EQE spectra in the long wavelength decrease gradually with reducing solar irradiance. When the solar irradiance is 50 W/m^2, the degradation in EQE of our solar cells is barely visible. The EQE spectra of the 50 W/m^2 one and the 500 W/m^2 one are nearly overlapped. Nevertheless, the decrease accelerates rapidly when the solar irradiance is lower than 50 W/m^2 and obvious EQE loss is observed. This phenomenon is mainly due to the depletion condition introduced by the positive oxide charges and the Si-Al work function difference, resulting in a high S_{eff} at the rear Si/SiO_2 interface under low illumination [33].

To understand how the solar irradiance affect the solar cell performances in the real application, we have evaluated the effective
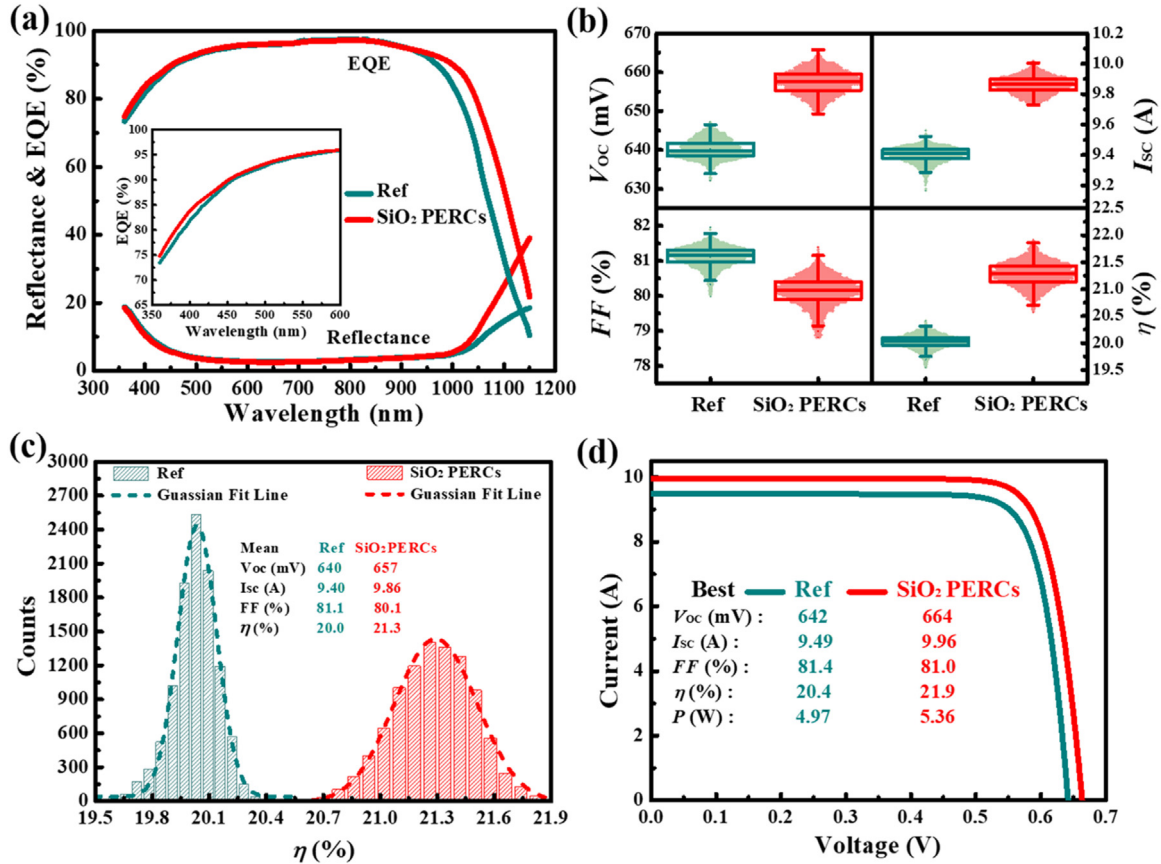
Fig. 6. Comparison of (a) reflectance and EQE spectra, (b) measured *I-V* parameters including V_{OC}, I_{SC}, *FF* and η, (c) distribution of η, and (d) *I-V* characteristics of the SiO₂ PERCs and the conventional Al-BSF solar cells.

electric energy production of our SiO₂ PERCs over a day in different seasons by calculations with taking Shanghai (121°, 31°) as an example of module location with a normal incidence. The detailed calculation processes are shown in the Supplementary information (Fig. S2). The relative low illumination response loss of our SiO₂ PERCs is illustrated in Fig. 7b. The impact of low illumination response on generating electric energy over a day seems to be extremely limited. The relative energy generation loss of our SiO₂ PERCs is less than 0.2%, demonstrating the excellent behaviors of the SiO₂ PERCs at low solar irradiance.

4. Conclusions

In summary, we have mass-produced high-efficiency p-type CZ-Si solar cells by employing SiO₂/SiNₓ:H stacks as the front passivation layers. The passivation quality of the front SiO₂/SiNₓ:H stacks has been evaluated from the J_{0e} of the solar cell precursors. It has been reduced from 90.5 fA/cm² to 62.3 fA/cm², resulting in a 10% reduction in blue loss. Attributed to the high performance of V_{OC} (645.6 mV) and I_{SC} (9.40 A), the average η of the thermal-oxidized p-type CZ-Si solar cells reaches 20.1%, which is 0.2% absolutely higher than that of the conventional Al-BSF solar cells. With a rational design of process integration, we have further presented a cost-effective way to fabricate high-
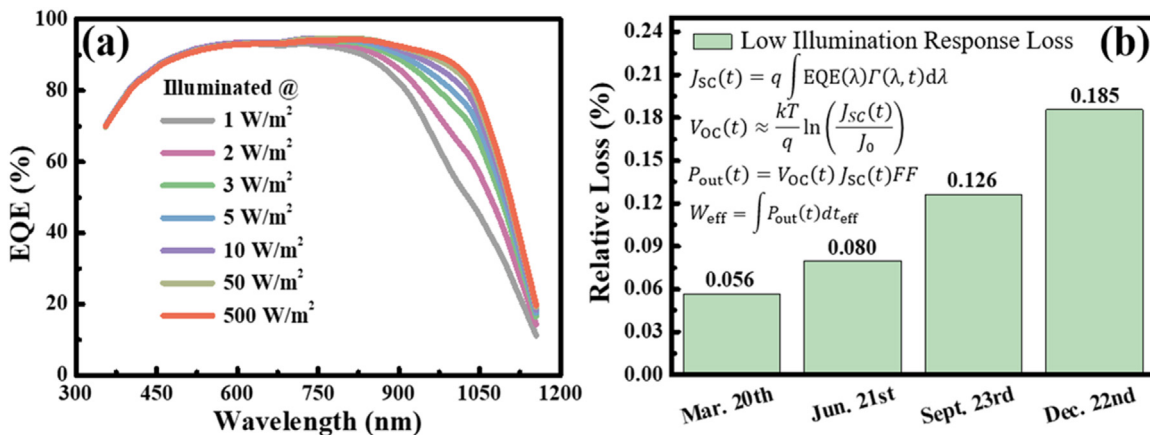

Fig. 7. (a) EQE spectra of the SiO₂ PERCs at the solar irradiance ranging from 1 to 500 W/m². (b) Relative low illumination response loss of the SiO₂ PERCs over a day.

efficiency SiO_2 PERCs at an existing production line. The introduction of SiO_2/SiN_x:H stacks on the rear surface effectively suppresses the penetration of evanescent waves in Al-BSF in the long wavelength, and hence more light can be reflected back into the silicon substrate and be re-absorbed. The rear SiO_2/SiN_x:H stacks also perform excellent surface passivation effects and a rather low S_{eff} of 26 cm/s is achieved after a post 700 °C annealing process. Consequently, the industrial SiO_2 passivated p-type CZ-Si PERCs possess high performances with average V_{OC} of 657 mV, I_{SC} of 9.86 A and η of 21.3%. Compared with the conventional Al-BSF solar cells, absolute 1.3% increment in η is achieved with the highest η of the SiO_2 PERCs over 21.9%. Finally, we have demonstrated that the impact of the low illumination response loss in the SiO_2 PERCs on generating electric energy is extremely limited, via a careful calculation with considering the variation of solar spectrum with time. The relative low illumination response (below $50\,W/m^2$) loss of our SiO_2 PERCs over a day is expected to be less than 0.2%, which removes the barriers in promoting SiO_2 passivation techniques in the PV industry. We believe that the present work is promising to realize high-efficiency silicon solar cells with low cost, especially for the existing production lines.

Acknowledgements

Appendix A. Supplementary material

Supplementary data associated with this article can be found in the online version at doi:10.1016/j.solmat.2019.01.038

References

[1] A.W. Blakers, A.H. Wang, A.M. Milne, J.H. Zhao, M.A. Green, 22.8% efficient silicon solar cell, Appl. Phys. Lett. 55 (1989) 1363.

[2] G. Dingemans, W.M.M. Kessels, Status and prospects of Al_2O_3-based surface passivation schemes for silicon solar cells, J. Vac. Sci. Technol. A 30 (2012) 040802.

[3] D.K. Simon, P.M. Jordan, I. Dirnstorfer, F. Benner, C. Richter, T. Mikolajick, Symmetrical Al_2O_3-based passivation layers for p- and n-type silicon, Sol. Energy Mater. Sol. Cells 131 (2014) 72.

[4] T. Dullweber, H. Hannebauer, S. Dorn, S. Schimanke, A. Merkle, C. Hampe, R. Brendel, Emitter saturation current densities of 22 fA/cm^2 applied to industrial PERC solar cells approaching 22% conversion efficiency, Prog. Photovolt. Res. Appl. 25 (2017) 509.

[5] W.L. Wu, Z.W. Zhang, F. Zheng, W.J. Lin, Z.C. Liang, H. Shen, Efficiency enhancement of bifacial PERC solar cells with laser doped selective emitter and double-screen-printed Al grid, Prog. Photovolt. Res. Appl. 26 (2018) 752.

[6] B. Hoex, J. Schmidt, P. Pohl, M.C.M. van de Sanden, W.M.M. Kessels, Silicon surface passivation by atomic layer deposited Al_2O_3, J. Appl. Phys. 104 (2008) 044903.

[7] B. Hoex, J.J.H. Gielis, M.C.M. van de Sanden, W.M.M. Kessels, On the c-Si surface passivation mechanism by the negative-charge-dielectric Al_2O_3, J. Appl. Phys. 104 (2008) 113703.

[8] G. Dingemans, P. Engelhart, R. Seguin, F. Einsele, B. Hoex, M.C.M. van de Sanden, W.M.M. Kessels, Stability of Al_2O_3 and Al_2O_3/a-SiN_x:H stacks for surface passivation of crystalline silicon, J. Appl. Phys. 106 (2009) 114907.

[9] H.B. Huang, J. Lv, Y.M. Bao, R.W. Xuan, S.H. Sun, S. Sneck, S. Li, C. Modanese, H. Savin, A.H. Wang, J.H. Zhao, 20.8% industrial PERC solar cell: ALD Al_2O_3 rear surface passivation, efficiency loss mechanisms analysis and roadmap to 24%, Sol. Energy Mater. Sol. Cells 161 (2017) 14.

[10] A.G. Meyer Burger, Deposition of backside AlO_x/SiN stacks and front SiN for high

[11] Z. Li, G. Xu, Y. Chen, Y. Yang, Z. Bian, Z. Feng, Q. Huang, Improved homogeneous emitter solar cells with double layer anti-reflection coatings, Energy Procedia 27 (2012) 402.

[12] T. Dullweber, J. Schmidt, Industrial silicon solar cells applying the passivated emitter and rear Cell (PERC) concept—a review, IEEE J. Photovolt. 6 (2016) 1366.

[13] M.A. Green, Silicon Solar Cells: Advanced Principles and Practice, Univ. of New South Wales, Sydney, 1995.

[14] B.W.H. van de Loo, H.C.M. Knoops, G. Dingemans, G.J.M. Janssen, M.W.P.E. Lamers, I.G. Romijn, A.W. Weeber, W.M.M. Kessels, "Zero-charge" SiO_2/Al_2O_3 stacks for the simultaneous passivation of n^+ and p^+ doped silicon surfaces by atomic layer deposition, Sol. Energy Mater. Sol. Cells 143 (2015) 450.

[15] H.B. Huang, C. Modanese, S.H. Sun, G.V. Gastrow, J.B. Wang, T.P. Pasanen, S. Li, L.C. Wang, Y.M. Bao, Z. Zhu, S. Sneck, H. Savin, Effective passivation of p^+ and n^+ emitters using $SiO_2/Al_2O_3/SiN_x$ stacks: surface passivation mechanisms and application to industrial p-PERT bifacial Si solar cells, Sol. Energy Mater. Sol. Cells 186 (2018) 356.

[16] Y.L. Chen, S.H. Zhong, M. Tan, W.Z. Shen, SiO_2 passivation layer grown by liquid phase deposition for silicon solar cell application, Front. Energy 11 (2017) 52.

[17] T. Jana, S. Mukhopadhyay, S. Ray, Low temperature silicon oxide and nitride for surface passivation of silicon solar cells, Sol. Energy Mater. Sol. Cells 71 (2002) 197.

[18] S. Mack, A. Wolf, A. Walczak, B. Thaidigsmann, E.A. Wotke, J.J. Spiegelman, R. Preu, D. Biro, Properties of purified direct steam grown silicon thermal oxides, Sol. Energy Mater. Sol. Cells 95 (2011) 2570.

[19] G. Dingemans, E. Kessels, Status and prospects of Al_2O_3-based surface passivation schemes for silicon solar cells, J. Vac. Sci. Technol. A 30 (2012) 1.

[20] N.M. Terlinden, G. Dingemans, V. Vandalon, R.H.E.C. Bosch, W.M.M. Kessels, Influence of the SiO_2 interlayer thickness on the density and polarity of charges in $Si/SiO_2/Al_2O_3$ stacks as studied by optical second-harmonic generation, J. Appl. Phys. 115 (2014) 033708.

[21] S. Mack, A. Wolf, C. Brosinsky, S. Schmeisser, A. Kimmerle, P. Saint-cast, M. Hofmann, D. Biro, Silicon surface passivation by thin thermal oxide/PECVD layer stack systems, IEEE J. Photovolt. 1 (2011) 135.

[22] S. Bordihn, P. Engelhart, V. Mertens, G. Kesser, High surface passivation quality and thermal stability of ALD Al_2O_3 on wet chemical grown ultra-thin SiO_2 on silicon, Energy Procedia 8 (2011) 654.

[23] S. Gatz, H. Hannebauer, R. Hesse, F. Werner, A. Schmidt, T. Dullweber, J. Schmidt, K. Bothe, R. Brendel, 19.4%-efficient large-area fully screen-printed silicon solar cells, Phys. Status Solidi RRL 5 (2011) 147.

[24] K.A. Munzer, J. Schone, M. Hein, A. Teppe, R.E. Schlosser, M. Hanke, J. Maier, K. Varner, S. Keller, P. Fath, Development and implementation of 19% rear passivation and local contact Centaurus technology, in: Proceedings of the 26th European Photovoltaic Solar Energy Conference, 2011, p. 2292.

[25] B. Vermang, P. Choulat, H. Goverde, J. Hozrel, J. John, R. Mertens, J. Poortmans, Integration of Al_2O_3 as front and rear surface passivation for large-area screen-printed p-type Si PERC, Energy Procedia 27 (2012) 325.

[26] Y.F. Zhuang, S.H. Zhong, H.Y. Xu, W.Z. Shen, Broadband spectral response of diamond wire sawn mc-Si solar cell with omnidirectional performance and improved appearance, Sol. Energy Mater. Sol. Cells 179 (2018) 372.

[27] D. Kane, R. Swanson, Measurement of the emitter saturation current by a contactless photoconductivity decay method, in: Proceedings of the 18th IEEE Photovoltaic Specialists Conference,1985, p. 578.

[28] Z.C. Holman, S.D. Wolf, C. Ballif, Improving metal reflectors by suppressing surface plasmon polaritons: a priori calculation of the internal reflectance of a solar cell, Light.: Sci. Appl. 2 (2013) e106.

[29] S.C. Shenzhen, PERC technology: Introduction to KOH system alkaline etching/polishing process, in: Proceedings 4th PERC Solar Cell and Bifacial Module Forum, 2018.

[30] G. Choi, N. Balaji, C. Park, J. Choi, S. Lee, J. Kim, M. Ju, Y. Lee, J. Yi, Optimization of PECVD-ONO rear surface passivation layer through improved electrical property and thermal stability, Vacuum 101 (2014) 22.

[31] A. Sproul, Dimensionless solution of the equation describing the effect of surface recombination on carrier decay in semiconductors, J. Appl. Phys. 76 (1994) 2851.

[32] A. Richter, S.W. Glunz, F. Werner, J. Schmidt, A. Cuevas, Improved quantitative description of Auger recombination in crystalline silicon, Phys. Rev. B 86 (2012) 165202.

[33] A.G. Aberle, S.J. Robinson, A.H. Wang, J.H. Zhao, S.R. Wenham, M.A. Green, High-efficiency silicon solar cells: fill factor limitations and non-ideal diode behavior due to voltage-dependent rear surface recombination velocity, Prog. Photovolt. Res. Appl. 1 (1993) 143.

efficient (bifacial) PERC solar cells in only one process system: MAiA 3in1, in: Proceedings of the 13th China SoG Silicon and PV Power Conference, 2017.